Research Paper

Electrospinning of Hydroxypropyl-β-cyclodextrin/ Polyvinylpyrrolidone Resveratrol-loaded Nanofibers: Preparation and Characterization

S. XIANG, H. W. TANG, J. ZHOU AND X. Z. LI[1]*

College of Materials Science and Engineering, Central South University of Forestry & Technology, [1]State Key Laboratory of Ecological Applied Technology in Forest Area of South China, Changsha 410004, China

In the present study, hydroxypropyl-β-cyclodextrin-polyvinylpyrrolidone-loaded resveratrol nanofibers were prepared via electrospinning to achieve higher water solubility of resveratrol. The hydroxypropyl-β-cyclodextrin-polyvinylpyrrolidone-loaded resveratrol electrospinning nanofibers were characterized with scanning electron microscopy, Fourier-transform infrared spectroscopy, Raman spectroscopy, differential scanning calorimetry, and ultraviolet irradiation test. Results obtained indicated successful encapsulation of resveratrol in hydroxypropyl-β-cyclodextrin-polyvinylpyrrolidone nanofibers, the diameter of the fiber could reach nanoscale and resveratrol existed in an amorphous state. The ultraviolet irradiation test demonstrated that the resveratrol electrospinning nanofibers were more stable than pure resveratrol when exposed to ultraviolet light. The solubility test indicated that the resveratrol electrospinning nanofibers had better water-solubility than pure resveratrol. Furthermore, the *in vitro* release study indicated that resveratrol electrospinning nanofibers achieved slow and sustained resveratrol release.

Key words: Resveratrol, electrospinning, water solubility, sustained release

Resveratrol (RS) is a natural flavonoid polyphenol compound that can mainly be found in grapes, mulberries, cranberries, peanuts, *Polygonum cuspidatum*[1], and other natural food sources[2]. Multiple biologic effects of RS have been reported, including cardiovascular protection[3], anticancer[4], antiinflammatory[5], antioxidant[6], antiviral[7] and immune regulation activities[8].

However, the poor water solubility of RS remains a major challenge for the application in the food industry[9]. This property renders RS unstable under ultraviolet irradiation, leading to low bioavailability *in vivo*. Therefore, the solubility and stability of RS must be enhanced to increase its application value and a large number of studies have addressed these questions.

On one hand, modifying the molecular structure of RS to create a water-soluble RS through site-selective enzymatic glycosylation[10] and water-soluble carbamate ester derivatives of RS[11], increased the water solubility of RS 380-fold. On the other hand, physical inclusion technologies can increase the stability of RS under light exposure. For example, α-cyclodextrin (CD)/RS host-guest complexes were reported to reduce the UV degradation and isomerization of trans-RS[12]. Similarly, RS-hordein nanoparticles were self-assembled via liquid-liquid dispersion[13], and the stability of RS in nanoparticles improved by 26 %. Moreover, RS encapsulated in a protein matrix[14] increased the stability of trans-RS to UV light exposure. Nevertheless, previous studies have ignored important details, such as the complex operation process, a number of uncontrollable factors, and the low encapsulation efficiency.

To overcome these disadvantages, nanofibers (NFs) loaded with bioactive substances based on electrospinning became a feasible alternative. The electrospinning fibers have received growing attention in several fields such as food engineering[15],

***Address for correspondence**
E-mail: RLXZ@163.com

Accepted 16 May 2019
Revised 19 January 2019
Received 30 October 2018
Indian J Pharm Sci 2019;81(4):618-625

biomedical engineering[16], sensing material[17], and catalytic carriers[18]. Bioactive substance-loaded NFs have a large specific surface area[19], enabling excellent encapsulation efficiency. Hydroxypropyl-β-CD (HP-β-CD) has a tubular structure[20], which is hydrophilic externally and lipophilic internally. This amphiphilic structure can solubilize insoluble substances, to improve water solubility and promote slow release and improved stability. In addition, HP-β-CD has relatively low relative surface activity and hemolytic activity, so it is safer to use and widely used in pharmacy[21]. Polyvinylpyrrolidone (PVP) is a water-soluble nitrogen-containing polymer that is non-toxic and has excellent biocompatibility for biologically active tissues[22].

In this study, RS-NFs were created with HP-β-CD/PVP as bioactive substance carriers by electrospinning, and we hypothesize that RS might be dispersed uniformly in the NFs and improve their water solubility. The NFs were characterized using scanning electron microscopy (SEM), Fourier-transform infrared spectroscopy (FTIR), differential scanning calorimetry (DSC) and ultraviolet irradiation tests. The solubility in water and *in vitro* release of the RS-NFs were tested as well.

MATERIALS AND METHODS

RS (98 %, Hengyuan Plant Biochemical Co., Ltd., China), HP-β-CD (Zhiyuan Biotechnology Co., Ltd., China), PVP, sodium dihydrogen phosphate, disodium hydrogen phosphate, anhydrous ethanol, and hydrochloric acid were of analytical grade and purchased from Sinopharm Chemical Reagent Co., Ltd., Shanghai, China.

The following provides the manufacturers of the equipment used, collector thermostatic magnetic heating stirrer (DF-101S, Yuhua Instrument Co., Ltd., China); ultrasonic cleaner (Meimei Ultrasonic Instrument Co., Ltd., China); electrospinning machine (Nanon-01A, MECC, Japan); rotating viscometer (NDJ-1, Shanghai Precision Instrument Co., Ltd., China); field emission SEM (Sigma HD, Zeiss, Germany); Cressington sputter coater (Cressington 108 Auto, Ted Pella, Inc., USA); Fourier-transform infrared spectrometer (Alpha, Bruker, Germany); Raman spectrometer (Renishaw microprobe RM2000, UK); differential scanning calorimeter (TA Instruments Q2000, USA); UV spectrophotometer (TU-1901, Purkinje General Instrument Co., Ltd. Beijing, China); dark box type UV automatic analyser (ZF-20C, Gucun electro-optical instrument factory, China); dissolution tester (RC-3, Xintianguang Analytical Instrument Technology Co., Ltd., China); dialysis bag (MD34, MWCO 8000D, Sigma Aldrich, China); desktop high speed centrifuge (TG16-WS, Ordinary Instrument and Meter Co., Ltd., China).

Preparation of RS-loaded nanofibers (RS-NFs):

RS-NFs were prepared using an electrospinning device. At room temperature, 0.5, 1, 1.5, 2 g HP-β-CD was dissolved in 10 g anhydrous ethanol to generate transparent polymer solution. Then, 5 % and 10 % RS with respect to HP-β-CD were mixed to ensure complete mixing. Two grams of PVP was added and dissolved. The solution was sonicated for 30 s. Then, a syringe loaded with the polymer solution was fitted with a 27 G steel needle and pumped at a flow rate of 0.2 ml/h. A voltage of 26.5 kV was applied, the tip-collector distance remained at 12.3 cm, and the nanofiber was collected through aluminum foil. The electrospinning conditions were kept at 25±5° with a humidity of approximately 50±5 % throughout the experiments.

Scanning electron microscopy (SEM):

Morphologies and dimensions of pure RS, 0, 5, and 10 % RS-NFs were observed using a field emission SEM (Sigma HD, Zeiss, Germany). All samples were sputter coated with gold (Cressington 108 Auto, Ted Pella, Inc., USA) at 0.06 mA for 20 s prior to the analysis. The average fiber diameters and their diameter distributions were determined by measuring 100 fibers for each image from three randomly selected SEM images using Nano Measurer (version 1.2) software.

Fourier-transform infrared (FT-IR) and Raman spectra:

The pure RS, 0, 5 and 10 % RS-NFs were tablet compressed with potassium bromide (KBr), and FT-IR of the NFs were recorded using an Alpha instrument (Bruker, Germany) at a resolution of 2 cm^{-1} with 32 scans over the wavelength range of 400-4000 cm^{-1}[23]. Raman spectroscopy was used to detect the atomic non-polar bond vibration of RS in the HP-β-CD/PVP NFs. The excitation wavelength was 785 nm, and the testing wavelength ranged from 300 to 3500 cm^{-1}.

Differential scanning calorimetry (DSC):

DSC (TA Instruments Q2000, USA) was performed under nitrogen atmosphere at a flow rate of 50 ml/min. About 5-10 mg pure RS, 0, 5 and 10 % RS-NFs were enclosed in the aluminium plate and heated from 30

to 350° with a heating rate of 10°/min[24]. Then the differential thermal scanning heating curves of samples were recorded.

Ultraviolet irradiation test:

RS (0.32 g) was precisely weighed and dissolved in 500 ml ethanol and the solution was diluted 100 times. Then, the solution was under the 254 nm UV light irradiation for 0, 5, 15, 30, 60, 120, and 240 min. Finally, the corresponding absorbance was measured. 5 and 10 % RS-NFs were treated in the same way and contained 0.32 g RS.

Water solubility properties:

The balance method has been widely used in research and high-purity material preparation, and has been used as a standard for calibrating new solubility measurement methods[25]. For example, Baka[26] measured the solubility of hydrochlorothiazide using the classic shake flask method. The balance method was used to determine the dissolution-related properties of RS-NFs.

Firstly, excessive 5 and 10 % RS-NFs were added into 1 ml H_2O, then heated to 37°, and shaken for three days after sealing. Furthermore, stirred it continuously or intermittently during the period to promote the dissolution of solids until it were as close as possible to the real solid-liquid equilibrium state. After setting, the saturated supernatant was collected and its composition was analysed by UV spectroscopy to obtain the solubility data of the solid solute in the liquid solvent.

Five and ten percent RS-NFs that contained 0.32 g RS were precisely weighed, dissolved in 500 ml ethanol and the solution was diluted 100 times. The solution was sonicated for 30 s and then, the absorbance was measured at 305 nm. Finally, the loading efficiency and encapsulation efficiency could be calculated using the following Eqn., loading efficiency (%) = weight of the RS in NFs/(weight of the HP-β-CD+PVP+feeding RS); encapsulation efficiency (%) = weight of the RS in NFs/weight of the feeding RS.

Five and ten percent RS-NFs were precisely weighed before and after freeze-drying, and the moisture content could be calculated with the Eqn., moisture content (%) = (weight before freeze drying–weight after freeze drying)/weight before freeze drying. The conditions for freeze-drying were as follows: cold trap temperature was –60°, sample drying temperature was 10°, drying time was 48 h, and drying pressure was 1 Pa.

***In vitro* release:**

In vitro dissolution studies were conducted according to the Chinese Pharmacopeia (2015 ED.) method II, which is a paddle method using a dissolution apparatus with sink conditions C<0.2 C s. 10 mg pure RS, 5 and 10 % RS-NFs, which contained 10 mg RS were dispersed in a specific amount of solvent and placed in a MD34 dialysis bag with the tongs closed at both ends. After that, dialysis bags were put into 500 ml appropriate solution. The appropriate solution was PBS (pH = 6.8, 7.4) and hydrochloric acid solution (pH = 1). The mixture was stirred at 50 rpm/min and 37°. At predetermined time intervals, samples of 5.0 ml were withdrawn from the dissolution medium and replaced with fresh medium via injectors to maintain a constant volume. The sample solutions were analysed at 305 nm on a UV spectrophotometer. Pure RS was used as a control.

Statistical analysis:

Each experiment was performed three times and the results are presented as the mean±standard deviation (SD). All data were collected and converted to graphs using Origin 8.0 software.

RESULTS AND DISCUSSION

In this study, single factor experiment was used to optimize the ratio of the excipients and the content of the RS in the electrospinning process. Among those, the considerations included the success of the spinning process, the state of the electrospun fiber and the state of the electrospinning solution. First of all, 5 groups of HP-β-CD:PVP were set up in different proportions, and the optimal ratio of HP-β-CD:PVP was determined by observing the success or failure of the spinning process and the morphology of the electrospun fibers. The results were shown in Table 1. After determining that the ratio of HP-β-CD:PVP was 1:2 (g/g), different amounts of RS were added, and the appropriate drug content was selected by the state of the electrospinning solution and the spinning effect. The results were shown in Table 2, and the RS content was determined to be 5 and 10 %, both of which were nanoscale, and the fiber morphology was good. Therefore, HP-β-CD:PVP is 1:2, and the RS content is 5 and 10 % were the optimal conditions.

Morphologies of the RS-NFs by electrospinning and the diameter distribution histogram are shown in fig. 1. SEM was performed to study RS with the irregular crystalline structure while the RS-NFs had

TABLE 1: FORMULATION OPTIMIZATION OF ELECTROSPINNING SOLUTION (HP-β-CD:PVP)

HP-β-CD:PVP	Spinning effect	Electrospun fiber state
0.5:2	Powdered product, not fibrous	—
1:2	Spinning succeeded	Smooth surface, uniform thickness, nanoscale
1.5:2	Spinning succeeded	Rough surface, uneven thickness, reaching micron level
2:2	The electrospinning solution was too viscous, the syringe does not move, and the spinning was unsuccessful	—

TABLE 2: FORMULATION OPTIMIZATION OF ELECTROSPINNING SOLUTION (RESVERATROL CONTENT)

Resveratrol content	Electrospinning solution state	Spinning effect
5 %	Clear and transparent light yellow solution	Spinning succeeded
10 %	Clear and transparent yellow solution	Spinning succeeded
15 %	White viscous substance in solution, incomplete dissolution	—

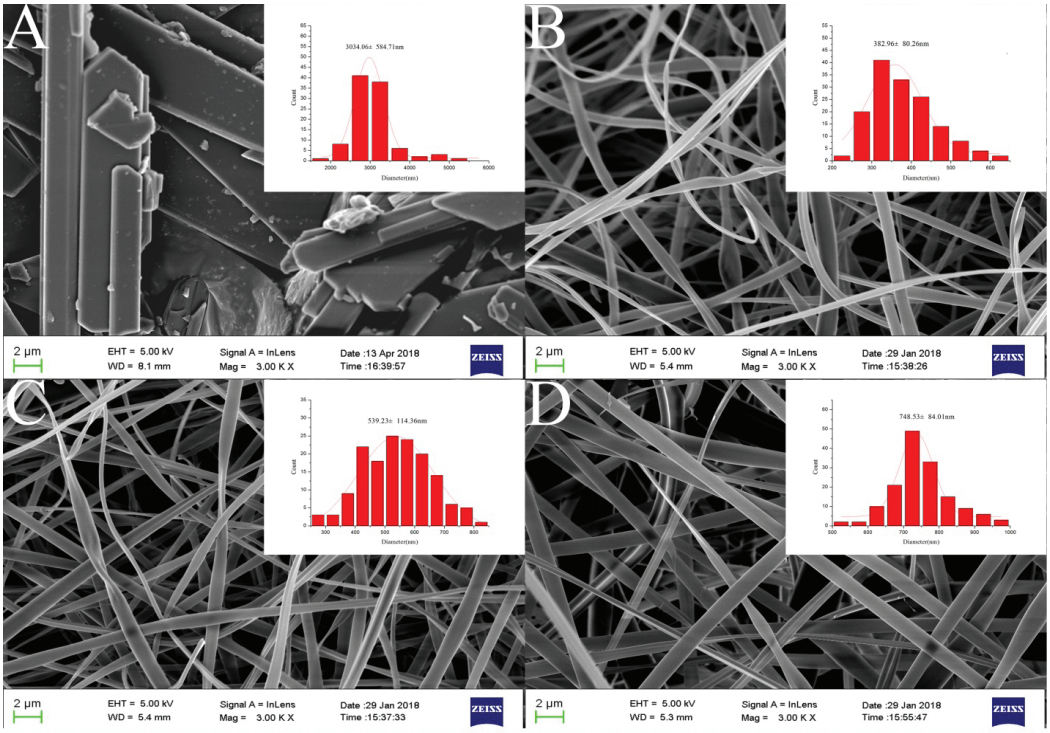

Fig. 1: SEM images and diameter distribution histogram of pure RS and RS-NFs
(A) Pure RS; (B) 0 % RS-NFs; (C) 5 % RS-NFs; (D) 10 % RS-NFs

diameters between 300 and 900 nm and were free of defects and homogeneous in composition.

When the HP-β-CD/PVP in anhydrous ethanol was electrospun, the solution viscosity was 1.42 Pa.s, which was lower than the critical spinning viscosity. At this time, it was difficult to maintain the continuity of the jet during the spinning process, and a stable fluid could not be formed. A small amount of adhesion or mass is formed on the receiving screen, and NFs with rough surface were generated with a diameter of about 380 nm (fig. 1B). The viscosity of the solution is one of the most important factors for the morphology of NFs[27]. Adding RS to the HP-β-CD/PVP solution could increase the viscosity, resulting in uniform smooth NFs without rough surfaces (fig. 1C). When the RS content was 5 %, the solution viscosity was 4.06 Pa.s, a good fiber morphology was formed, the fiber diameter distribution was uniform, and the average diameter reaches 500 nm. The reason was that as the concentration of the solution increases, the viscosity of the solution also increased rapidly, preventing the jet from deforming, thereby forming a uniform fiber. When the RS content was 10 %, the solution viscosity was 8.17 Pa·s. As the weight ratio of RS increased from 5 to 10 %, the NF diameters gradually increased from 500 to 750 nm (fig. 1D). When the concentration

and viscosity of the electrospinning solution were low, only polymer beads could be obtained. When the concentration and viscosity of the solution were higher than a critical value, the solution jet was stretched by the electric force and had a long relaxation time due to the increase of the degree of entanglement between the molecular chains. Furthermore, the entangled molecular chain was oriented along the jet axial direction. The formation of the continuous electrospinning fiber structure was a result of the effective suppression of partial molecular chain breakage in the jet. When the molecular chains of the solution were highly entangled, the force was stretched more evenly and the jet whipped due to surface charge and electric field force. After the solvent evaporated, the solvent solidified into fibers, while increasing the fiber diameter. The morphologic observations suggest that pure RS with irregular crystal structure turned into smooth, uniform fibers through electrospinning.

The FTIR spectrum showed three characteristic peaks of pure RS, which corresponded to the three typical strong bands in fig. 2, 1383.85 cm^{-1} could be assigned to the C=O stretching vibration, 1586.53 cm^{-1} could be assigned to the C=C olefinic bond stretching vibration, and 1606.21 cm^{-1} could be assigned to the C=C aromatic double bond stretching vibration. Nevertheless, the strength of the characteristic peak decreased or disappeared clearly in the RS-NFs. It is worth mentioning that with the increase of the content of RS, the infrared characteristic absorption peak showed no obvious difference between individual RS-NFs. Therefore, an additional analysis of this phenomenon was conducted, using the Raman spectrum because the infrared and Raman spectra are complementary[28].

There was high intensity at 1616 cm^{-1}, showing that RS were clearly detected in RS-NFs (fig. 3A) and with the amount of RS increase, the characteristic peak became more pronounced (fig. 3B). Moreover, the changes of material characteristic peak proved that the formation of the inclusion compound and the characteristic peaks of RS and HP-β-CD/PVP in the spectrum of RS-NFs demonstrated the successful loading of RS into RS-NFs.

DSC analysis was performed to investigate the thermal stability of RS-NFs. Fig. 4 shows the DSC curves. This shows that the pure RS powder had a sharp endothermic peak at approximately 270.08°, which corresponds to the decomposition temperature of RS[29]. The RS-NFs showed no distinct thermal peak at this temperature. On the DSC chart, the size and position of the peak reflected the change in the microscopic properties of the material, and the thermal stability was poor when the endothermic peak is apparent. However, the stable

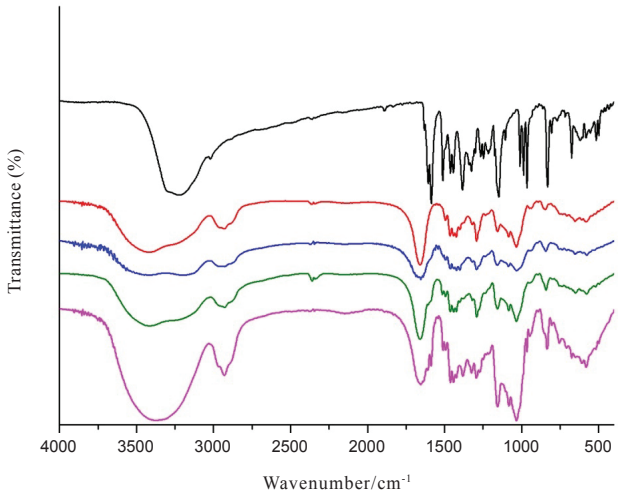

Fig. 2: FT-IR spectra of pure RS and RS-NFs
(—) RS, (—) 0% RS-NFs, (—) 5 % RS-NFs, (—) 10 % RS-NFs, (—) physical mixture

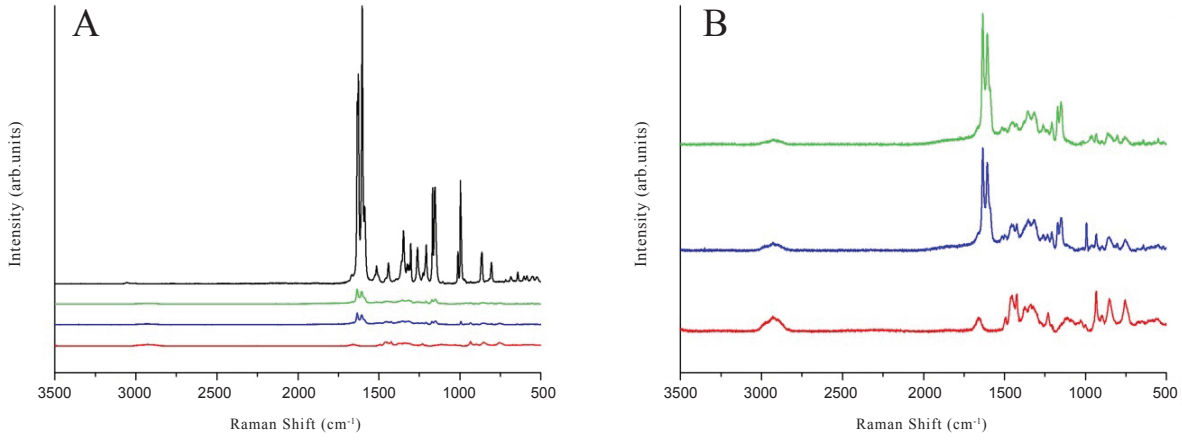

Fig. 3: Raman spectrums of pure RS and RS-NFs
(—) RS, (—) 0% RS-NFs, (—) 5 % RS-NFs, (—) 10 % RS-NFs

DSC curve of RS-NFs was relatively flat, with few endothermic peaks appearing or low endothermic peaks, indicating that the RS-NFs had good thermal stability. This illustrated that RS and HP-β-CD/PVP carrier formed a blend, and there were no RS crystals in RS-NFs.

The fig. 5 shows that the concentration of pure RS decreased by 56 % while the concentration of RS-NFs decreased by 38 % under ultraviolet irradiation during 4 h. This illustrates that the RS-NFs can slow down the speed of the RS light decomposition and the RS-NFs were more stable than pure RS to light.

The solubility in water of 5 % RS-NFs was 19.52 mg/ml, which was 650 times higher than the solubility of pure RS, while the solubility in water of 10 % RS-NFs was 18.2 mg/ml, which was 605 times higher than the solubility of pure RS. With the increase of the content of pure RS, the solubility in water of the RS-NFs decreased gradually. This phenomenon was caused by the relative decline of HP-β-CD, while HP-β-CD had good solubility in water.

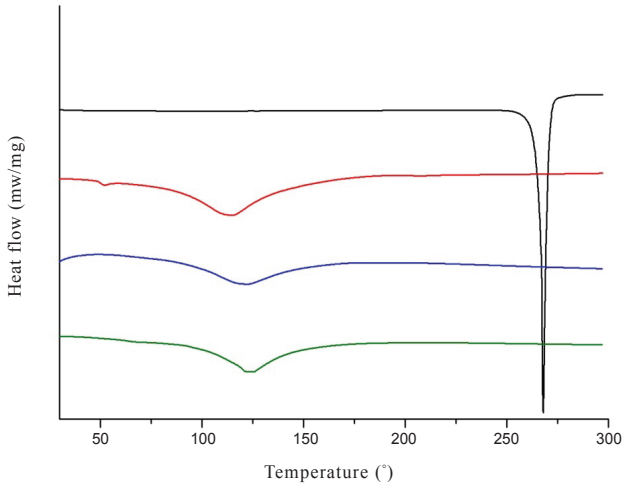

Fig. 4: DSC curves of pure RS and RS-NFs
(—) RS, (—) 0% RS-NFs, (—) 5 % RS-NFs, (—) 10 % RS-NFs

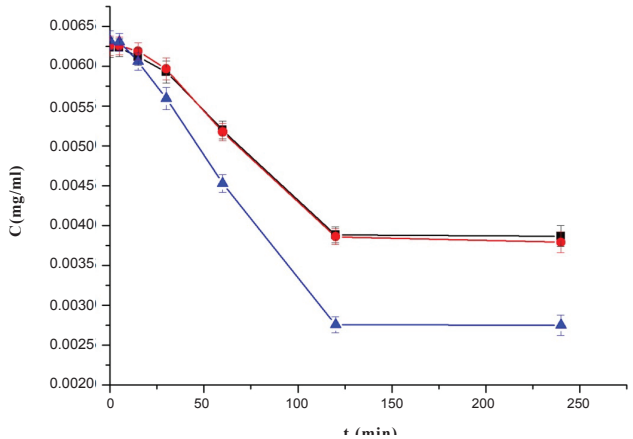

Fig. 5: Ultraviolet irradiation curves of pure RS and RS-NFs
(—■—) 10 % RS-NFs, (—●—) 5 % RS-NFs, (—▲—) RS

The loading efficiencies of 5 % RS-NFs and 10 % RS-NFs were 4.877 and 9.738 %, respectively, and their encapsulation efficiencies were 97.54 and 97.38 %, respectively. Due to the large specific surface area of NFs, RS-NFs had excellent encapsulation efficiency. Moreover, the moisture contents of 5 % RS-NFs and 10 % RS-NFs were 4.15 and 4.87 %, respectively; therefore, the moisture content of RS-NFs was low and it was easy to preserve[30].

As shown in fig. 6, the RS-NFs showed a prominent sustained release behaviour in solutions at pH 7.4 and pH 6.8 within 24 h (fig. 6A and B). However, the RS-NFs show less obvious sustained release in pH 1 solution within 4 h (fig. 6C). The pH 1 solution simulated gastric juice and the pH 7.4 and 6.8 solutions simulated intestinal juice. The average residence time of food in the stomach is about 4 to 5 h, while it is 10 to 20 h in the intestine[31]. The intestinal juice of people with gastrointestinal diseases is more acidic than the intestinal juice of healthy people. Therefore, the test demonstrated that RS-NFs have a certain sustained-release effect by combining the first 4 h of simulated gastric fluid and the subsequent 20 h of simulated intestinal fluid release behaviour.

RS has low solubility in water, resulting in low bioavailability, and its application is limited. In addition, the indications for RS are characterized by frequent onset and long-term use, and RS is absorbed in all stages of the intestine. Therefore, RS is suitable as a sustained-release preparation in terms of improving bioavailability, reducing the amount of drug used and the number of administrations, reducing toxic side effects, and increasing patient compliance.

In the current study, HP-β-CD/PVP loading RS-NFs were fabricated via electrospinning. The electrospinning process dispersed RS well into the HP-β-CD/PVP and formed a homogeneous NF structure, resulting in higher solubility in water, which is 650 times higher than pure RS. This work enables inferences about other bioactive substance that are structurally similar to RS, thus promoting their water solubility.

Electrospinning technology has a good application in tissue engineering, drug transportation and so on. Electrospun fibers has the advantages of large specific surface area, high drug loading and controllable drug release, and has good application prospects in drug delivery, they can be used to carry antibiotics, anticancer

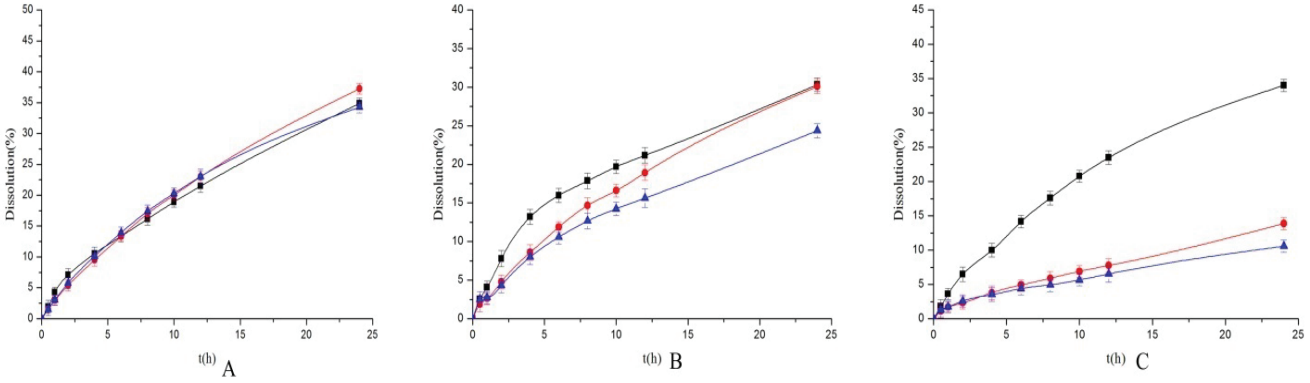

Fig. 6: *In vitro* release curves of pure RS and RS-NFs in different solvent systems (—■—) RS, (—●—) 5 % RS-NFs, (—▲—) 10 % RS-NFs; A: pH 1, B: pH 6.8, C: pH 7.4

drugs, and other biological agents such as proteins and DNA by coating and embedding. Therefore, RS-NFs are beneficial to increase the water solubility of RS, improve bioavailability and application value in the medical field. How to control the diameter of electrospun fibers to tens or even a few nanometers is a difficult problem, and researchers need to constantly explore this mystery.

Acknowledgements:

This work was supported by the National Key R&D Program Fund of China (2016YFD0600805). I would like to express my deepest gratitude to Miss Li for letting me be her master student. Special thanks to Mr. Zhou for his great help and support in my experiments and article modification. I am also grateful to the Central South University of Forestry Technology for providing the research platform. Finally, I extend my sincere gratitude to my family and friends.

REFERENCES

1. Gong YJ, Wang W, Zeng BQ, Ji-Lie LI, Yao YF. Biotransformation of polydatin from *Polygonum cuspidatum* by high cellulose-yield microbial. J Cent South Univ T 2010;30(9):190-201.
2. Macedo RC, Vieira A, Marin DP, Otton R. Effects of chronic resveratrol supplementation in military firefighters undergo a physical fitness test--a placebo-controlled, double blind study. Chem Biol Interact 2015;227:89-95.
3. Wu Z, Huang A, Yan J, Liu B, Liu Q, Zhang J, *et al*. Resveratrol Ameliorates Cardiac Dysfunction by Inhibiting Apoptosis via the PI3K/Akt/FoxO3a Pathway in a Rat Model of Diabetic Cardiomyopathy. J Cardiovasc Pharmacol 2017;70(3):184-93.
4. Nivelle L, Hubert J, Courot E, Jeandet P, Aziz A, Nuzillard JM, *et al*. Anti-Cancer Activity of Resveratrol and Derivatives Produced by Grapevine Cell Suspensions in a 14 L Stirred Bioreactor. Molecules 2017;22(3):474-87.
5. Lanzilli G, Cottarelli A, Nicotera G, Guida S, Ravagnan G, Fuggetta MP. Anti-inflammatory Effect of Resveratrol and Polydatin by *In vitro* IL-17 Modulation. Inflammation 2012;35(1):240-8.
6. Yao J, Wang JY, Liu L, Li YX, Xun AY, Zeng WS, *et al*. Anti-oxidant Effects of Resveratrol on Mice with DSS-induced Ulcerative Colitis. Arch Med Res 2010;41(4):288-94.
7. Li C, Fang JS, Lian WW, Pang XC, Liu AL, Du GH. *In vitro* anti-viral effects and 3D QSAR study of resveratrol derivatives as potent inhibitors of influenza H1N1 neuraminidase. Chem Biol Drug Des 2015;85(4):427-38.
8. Lai X, Pei Q, Song X, Zhou X, Yin Z, Jia R, *et al*. The enhancement of immune function and activation of NF-κB by resveratrol-treatment in immunosuppressive mice. Int Immunopharmacol 2016;33:42-7.
9. Hu C, Wang Q, Ma C, Xia Q. Non-aqueous self-double-emulsifying drug delivery system: A new approach to enhance resveratrol solubility for effective transdermal delivery. Colloids Surf A 2016;489:360-9.
10. Lepak A, Gutmann A, Kulmer ST, Nidetzky B. Creating a Water-Soluble Resveratrol-Based Antioxidant by Site-Selective Enzymatic Glucosylation. Chembiochem 2015;16(13):1870-4.
11. Mattarei A, Carraro M, Azzolini M, Paradisi C, Zoratti M, Biasutto L. New water-soluble carbamate ester derivatives of resveratrol. Molecules 2014;19(10):15900-17.
12. Allan KE, Lenehan CE, Ellis AV. UV Light Stability of α-Cyclodextrin/Resveratrol Host–Guest Complexes and Isomer Stability at Varying pH. Aust J Chem 2009;62(8):921-6.
13. Xiao G, Yin T, Fei H. Light Stability,Controlled-release and Antioxidation of Resveratrol-hordein Composite Nanoparticles. Chem J Chin Univ 2015;36(9):1707-12.
14. Koga CC, Andrade JE, Ferruzzi MG, Lee Y. Stability of Trans-Resveratrol Encapsulated in a Protein Matrix Produced Using Spray Drying to UV Light Stress and Simulated Gastro-Intestinal Digestion. J Food Sci 2016;81(2):C292-C300.
15. Wongsasulak S, Patapeejumruswong M, Weiss J, Supaphol P, Yoovidhya T. Electrospinning of food-grade nanofibers from cellulose acetate and egg albumen blends. J Food Eng 2010;98(3):370-6.
16. Tan R, Yang X, Shen Y. Robot-aided electrospinning toward intelligent biomedical engineering. Robotics Biomim 2017;4(1):17-9.
17. Du HY, Wang J, Yu P, Yu NS, Sun YH, Tian JL. Investigation of gas sensing materials tin oxide nanofibers treated by oxygen plasma. J Nanopart Res 2014;1(2):1-10.
18. Duan G, Koehn-Serrano M, Greiner A. Highly Efficient Reusable Sponge-Type Catalyst Carriers Based on

Short Electrospun Fibers. Macromol Rapid Comm 2017;38(3):1600511.
19. Ignatova M, Rashkov I, Manolova N. Drug-loaded electrospun materials in wound-dressing applications and in local cancer treatment. Expert Opin Drug Del 2013;10(4):469-83.
20. Zhang D, Pan X, Wang S, Zhai Y, Guan J, Fu Q, *et al*. Multifunctional Poly (methyl vinyl ether-co-maleic anhydride)-graft-hydroxypropyl-β-cyclodextrin Amphiphilic Copolymer as an Oral High-Performance Delivery Carrier of Tacrolimus. Mol Pharm 2015;12(7):2337-51.
21. Linares MS, Longhi MR. Effects of hydroxypropyl-beta-cyclodextrin on the chemical stability of a naphthoquinone in aqueous solutions. Pharmazie 2003;58(1):32-7.
22. Reddy N, Nama D, Yang Y. Polylactic acid/polypropylene polyblend fibers for better resistance to degradation. Polym Degrad Stab 2015;93(1):233-41.
23. Kumpugdee-Vollrath M, Ibold Y. Increasing Solubility of Poorly Water Soluble Drug Resveratrol by Surfactants and Cyclodextrins. Adv Mater Res 2011;418-420:2231-34.
24. Ansari KA, Vavia PR, Trotta F, Cavalli R. Cyclodextrin-Based Nanosponges for Delivery of Resveratrol:In VitroCharacterisation, Stability, Cytotoxicity and Permeation Study. AAPS PharmSciTech 2011;12(1):279-86.
25. Grant DJW, Higuchi T. Solubility behavior of organic compounds. 1st ed. Hoboken, New Jersey, United States: Wiley-Interscience; 1990. p. 221-43.
26. Baka E, Tak K. Study on standardization of shake-flask solubility determination method. Eur J Pharm Sci 2007;32(1):S23-4.
27. Petras D, Slobodian P, Pavlínek V, Sáha P, Kimmer D. The Effect of PVAc Solution Viscosity on Diameter of PVAc Nanofibres Prepared by Technology of Electrospinning. Novel Trends in Rheology IV. AIP Conf Proc 2011;1375:312-9.
28. Peterson KI, Pullman DP. Determining the Structure of Oxalate Anion Using Infrared and Raman Spectroscopy Coupled with Gaussian Calculations. J Chem Edu 2016;93(6):1130-3.
29. Xiao ZB, Zhao YN, Liu YL, Song K, Chen S. Study on Melting Point. Thermal Stability and Decomposition Kinetics of Resveratrol and Piceid by the Non-isothermal Analysis. J Instrum Anal 2015;34(10):1119-25.
30. Fresta M, Cilurzo F, Cosco D, Paolino D. Innovative Drug Delivery Systems for the Administration of Natural Compounds. Curr Bioact Comp 2007;3(4):262-77.
31. Singh S, Singh RP. Gastric digestion of foods: Mathematical modeling of flow field in a human stomach. In: Aguilera JM, Barbosa-Canovas GV, Simpson R, Welti-Chenas J, Bermudez-Aguirre D, editors. Food engeneering interfaces. New York: Springer; 2010. p. 455-67.